FERROELECTRICS

Interfacial ferroelectricity by van der Waals sliding

M. Vizner Stern[1], Y. Waschitz[1], W. Cao[2], I. Nevo[1], K. Watanabe[3], T. Taniguchi[3], E. Sela[1], M. Urbakh[2], O. Hod[2], M. Ben Shalom[1]*

Despite their partial ionic nature, many-layered diatomic crystals avoid internal electric polarization by forming a centrosymmetric lattice at their optimal van der Waals stacking. Here, we report a stable ferroelectric order emerging at the interface between two naturally grown flakes of hexagonal boron nitride, which are stacked together in a metastable non-centrosymmetric parallel orientation. We observe alternating domains of inverted normal polarization, caused by a lateral shift of one lattice site between the domains. Reversible polarization switching coupled to lateral sliding is achieved by scanning a biased tip above the surface. Our calculations trace the origin of the phenomenon to a subtle interplay between charge redistribution and ionic displacement and provide intuitive insights to explore the interfacial polarization and its distinctive "slidetronics" switching mechanism.

The ability to locally switch a confined electrical polarization is a key functionality in modern technologies, where storing and retrieving a large volume of information is vital (*1*). The need to reduce the dimensions of individually polarized domains, from the ~100-nm^2 scale (*2*, *3*) toward the atomic scale, is rising (*4*). The main challenges involve long-range dipole interactions, which tend to couple the individual domain polarization orientations (*5*). Likewise, surface effects and external strains that are difficult to control become dominant once the surface-to-volume ratio increases (*6*). To overcome these challenges, one can consider layered materials, such as hexagonal boron nitride (*h*-BN) and transition-metal dichalcogenides (TMDs), where the bulk volume can be reduced to the ultimate atomic-thickness limit, whereas the crystalline surface remains intact (*7*). However, it is rare to find a spontaneous net electric polarization in two dimensions (2D) that is sufficiently large to read and write under ambient conditions (*8*–*10*). Furthermore, in naturally grown *h*-BN and TMD crystals, polarization is eliminated by the formation of a centrosymmetric van der Waals (vdW) structure that is lower in energy than other metastable stacking configurations. Here, we break this symmetry by controlling the twist angle between two *h*-BN flakes and find an array of permanent and switchable polarization domains at their interface. The polarization is oriented normal to the plane, and its amplitude is in good agreement with previous first-principle predictions for a two-layered system (*11*) and with our detailed multilayer calculations.

To identify which stacking modes can carry polarization, we present in Fig. 1A six different high-symmetry configurations of bilayer *h*-BN. The stacking configurations are divided into two groups termed "parallel" and "antiparallel" twist orientations (*12*); within each group, a relative lateral shift by one interatomic distance switches the stacking configuration in a cyclic manner. Typically, the crystal grows in the optimal antiparallel (AA') configuration with full overlap between nitrogen (boron) atoms of one layer and boron (nitrogen) atoms of the adjacent layer (*13*). In the parallel twist orientation, however, the fully eclipsed configuration (AA) is unstable because it forces pairs of bulky nitrogen atoms atop each other, resulting in increased steric repulsion (*14*). Instead, a lateral interlayer shift occurs to a metastable AB stacking with only half of the atoms overlapping, whereas the other half are aligned with the empty centers of the hexagons in the adjacent layer (*15*, *16*). The AB and BA stacking form equivalent lattice structures (only flipped), and all depicted antiparallel configurations (AA', AB1', AB2') are symmetric under spatial inversion.

To explore these different configurations, we artificially stamped two exfoliated *h*-BN flakes on top of each other, each consisting of a few AA' stacked layers, with a minute twist angle between the otherwise parallel interfacial layers (*17*). The small twist imposes interlayer translations that evolve continuously and form a moiré pattern owing to the underlying crystal periodicity (Fig. 1B). In this rigid lattice picture,

[1]School of Physics and Astronomy, Tel Aviv University, Israel. [2]Department of Physical Chemistry, School of Chemistry, The Raymond and Beverly Sackler Faculty of Exact Sciences and The Sackler Center for Computational Molecular and Materials Science, Tel Aviv University, Tel Aviv 6997801, Israel. [3]National Institute for Material Science, Tsukuba, Japan.
*Corresponding author. Email: moshebs@tauex.tau.ac.il

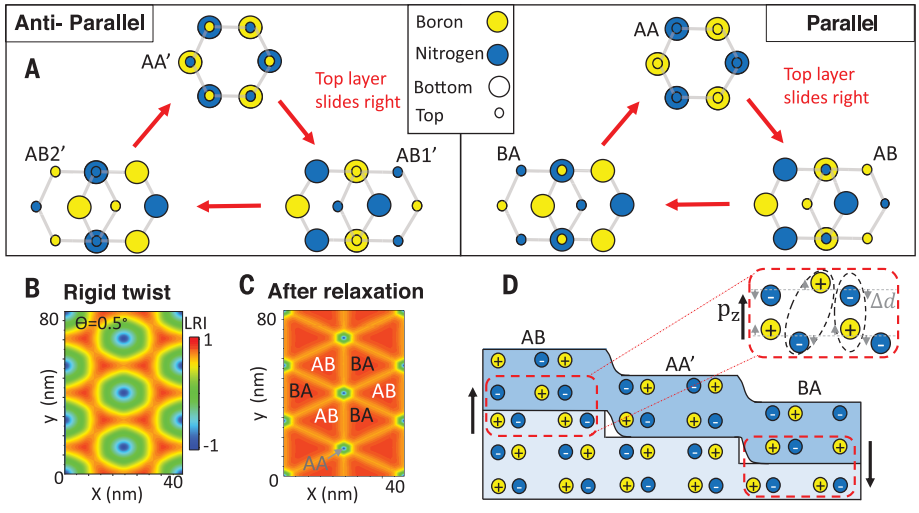

Fig. 1. High-symmetry interlayer stacking configurations. (**A**) Top view illustration of two layers. For clarity, atoms of the top layer are represented by smaller circles. Within each group of parallel or antiparallel twist orientations, a relative lateral shift by one lattice spacing results in a cyclic switching between three high-symmetry stacking configurations. (**B**) Calculated local-registry index (LRI) map of the atomic overlaps (*17*) in a rigid structure made of two *h*BN layers stacked with a twist angle of 0.5°. Blue regions correspond to AA stacking, whereas AB/BA stacking appears in orange (LRI = 0.86). (**C**) Calculated LRI map after geometry relaxation of the structure presented in (B). Large domains of uniform untwisted AB/BA stacking appear, at the expense of the preoptimized AA regions. The twist is accumulated in smaller AA-like regions and in the ~10-nm-wide incommensurate domain walls (bright lines); see fig. S3 and (*17*) for further discussion. (**D**) Cross-sectional illustration of two few-layered flakes (blue and light blue regions mark the top and bottom flakes, respectively) of naturally grown *h*-BN (AA'), which are stacked with no twist. Plus (minus) signs mark boron (nitrogen) sites. A topographical step of a single-layer switches between parallel and antiparallel stacking orientations at the interface between the two flakes. Vertical charge displacements in eclipsed/hollow pairs (vertical/diagonal ellipses) and the resulting net polarization P_z are marked by arrows.

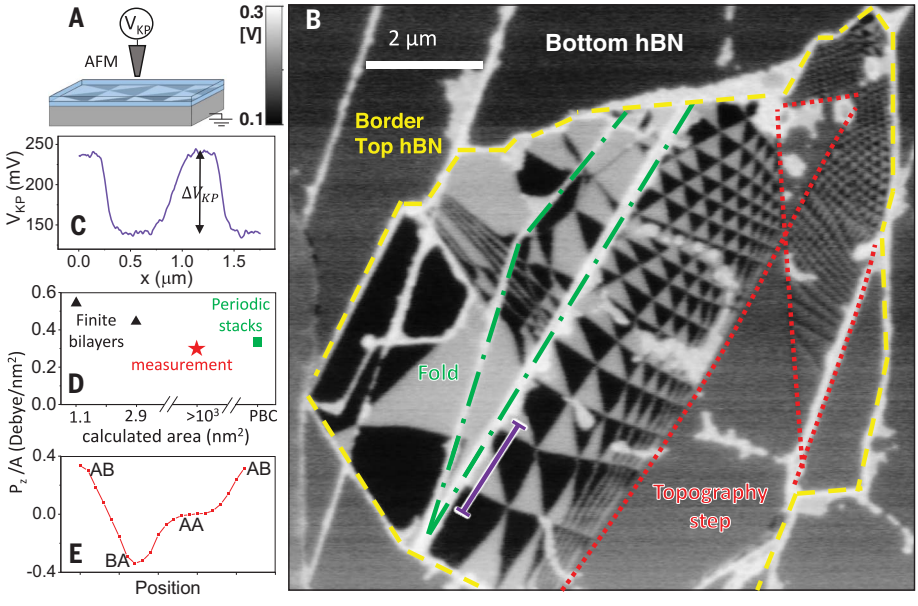

Fig. 2. Direct measurement of interfacial polarization. (**A**) Illustration of the experimental setup. An atomic force microscope is operated in Kelvin-probe mode to measure the local potential modulation, V_{KP}, at the surface of two 3-nm-thick *h*-BN flakes, which are stacked with a very small twist angle. (**B**) V_{KP} map showing oppositely polarized domains of AB/BA stacking (black and white), ranging in area between ~0.01 and 1 μm^2 and separated by sharp domain walls. (**C**) Surface potential measured along the purple line marked in (B) by first-harmonic KPFM. (**D**) DFT calculations of the polarization, P_z, per unit area obtained for finite *h*-BN bilayer flakes of different lateral dimensions (1.1 and 2.9 nm^2, black triangles) and for laterally periodic stacks made of 2 to 10 layers (marked as PBC, green square). The red star marks the polarization value evaluated from the measured ΔV_{KP} data. (**E**) Calculated polarization for different interlayer shifts.

the three nearly commensurate stacking configurations (AB, BA, AA) appear at adjacent positions in space. Notably, this picture breaks for a sufficiently small twist angle as a result of structural relaxation processes, as shown by our molecular dynamics calculation based on dedicated interlayer potentials (Fig. 1C) (*17*, *18*). Instead, the system divides into large domains of reconstructed commensurate AB and BA stackings separated by sharp incommensurate domain walls that accommodate the global twist (fig. S3, A and B) (*19*–*22*). Notably, near the center of the extended commensurate domains, perfectly aligned configurations are obtained with no interlayer twist. In the experiments, we also introduce a topographic step at the interface between the flakes. A step thickness of an odd number of layers guarantees antiparallel stacking (AA', AB1', or AB2') on one side and parallel stacking (AA, AB, or BA) on its other side (Fig. 1D). Thus, one can compare all possible configurations at adjacent locations in space.

To measure variations in the electrical potential, V_{KP}, at surface regions of different stacking configurations, we place the *h*-BN sandwich on a conducting substrate (Si/SiO_2, graphite, or gold) and scan an atomic force microscope (AFM) operated in a Kelvin probe mode (KPFM) (Fig. 2A) (*17*). The potential map above the various stacking configurations is shown in Fig. 2B. We find clear domains (black and white) of constant V_{KP}, extending over areas of several square micrometers, which are separated by narrow domain walls. Dark gray areas of average potential are observed above (i) positions where only one *h*-BN flake exists (outside the dashed yellow line); (ii) above two flakes but beyond the topographic step marked by dashed red lines in Fig. 2B (and topography map fig. S2), as expected; and (iii) beyond topographic folds that can further modify the interlayer twist angle (dashed green lines). These findings confirm that white and black domains correspond to AB and BA interfacial stacking that host a permanent out-of-plane electric polarization. Such polarization is not observed at the other side of the step, where centrosymmetric AA', AB1', AB2' configurations are obtained, or at the AA configuration expected at domain-wall crossings (blue dots in Fig. 1C). Sufficiently far from the domain walls (toward the center of each domain), a constant potential is observed with a clear difference ΔV_{KP} between the AB and BA domains, as shown in Fig. 2C. Whereas KPFM measurement nullifying the tip response at the electric bias frequency gives an underestimated potential difference of ΔV_{KP}~100 mV because of averaging contributions from the tip's cantilever (*17*), more quantitative measurements obtained through sideband tip excitations yield ΔV_{KP} values ranging between 210 and 230 mV for both closed-loop scans and local open-loop measurements (fig. S1). Similar values are measured for several samples with different substrate identities and various thicknesses of the top *h*-BN flake (for flakes thicker than 1 nm), and when using different AFM tips. These findings confirm that ΔV_{KP} is an independent measure of the intrinsic polarization of the system that, in turn, is confined within a few interfacial layers.

Although our force field calculations for slightly twisted bilayer *h*-BN show a uniform triangular lattice of alternating AB and BA stacked domains (Fig. 1C), in the experiment we observe large variations in their lateral dimensions and shape. This indicates minute deviations in the local twist, which are unavoidable in the case of small twist angles (*19*–*22*). Specifically, the ~1-μm^2 domains in the left part of Fig. 2B correspond to a global twist of less than 0.01° (*23*). In addition, any external perturbation to the structure, caused either by transferring it to a polymer, heating, or directly pressing it with the AFM tip, usually resulted in a further increase in domain size. In a few cases, high-temperature annealing resulted in a global reorientation to a single domain flake, many micrometers in dimensions. This behavior confirms the metastable nature of the AB/BA stacking mode, as well as the possible superlubric nature of the interface (*24*, *25*). At the other extreme, much smaller domains are observed in the top right-hand section of Fig. 2B. The smallest triangle edge that we could identify over many similar flakes was 60 nm in length, which corresponds to a twist angle of 0.24°. We therefore conclude that, below this angle, atomic reconstruction to create untwisted domains is energetically favored. Naturally, this constitutes a lower bound on the maximal angle for domain formation as smaller domains below our experimental resolution may form at larger twist angles.

To trace the microscopic origin of the measured polarization, we performed a set of density functional theory (DFT) calculations on finite bilayer and quad-layer *h*-BN flakes. For the finite bilayer calculations, we constructed two model systems, where hydrogen passivated *h*-BN flakes of either 1 or 3nm^2 surface area are stacked in the AB stacking mode (fig. S4). The calculated polarizations per unit area, P_z/A, of these systems were 0.55 and 0.45 Debye/nm^2, respectively (black triangles in Fig. 2D), pointing perpendicular to the interface only (table S1). Because edge effects may influence the results of such finite system calculations (*17*) (fig. S4), we performed complementary laterally periodic system calculations at various thicknesses. The detailed methods used for these calculations are discussed in (*17*). For the AB stacked periodic

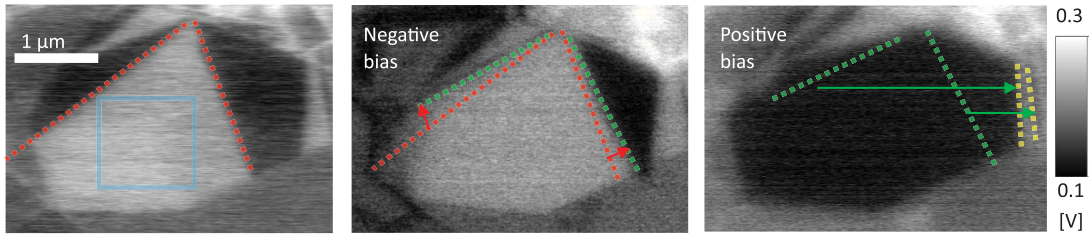

Fig. 3. Dynamic flipping of polarization orientation by domain-wall sliding. Kelvin-probe maps measured consecutively from left to right above a particular flake location showing domains of up (white) and down (black) polarizations. The middle image was taken after biasing the tip by a fixed DC voltage of −20 V and scanning it above the blue square region shown on the left-hand image. Then the tip was biased by 10 V and scanned again over the same region before taking the right-hand image. Consecutive domain-wall positions are marked by dashed red, green, and yellow lines. Larger white (black) domains appear after positive (negative) bias scans as a result of domain-wall motion beyond the scan area. Note that the number of domain walls is apparently not altered.

bilayer, we find a polarization of $P_z/A = 0.33$ Debye/nm^2, changing by only 10% when including additional two and eight AA' stacked layers above and below the AB stacked interface (see Fig. 2D and fig. S7). Adding more AB-stacked layers, however, reveals a linear increase of the calculated polarization with the number of added interfaces (fig. S9). The latter is a highly appealing control mechanism to engineer the magnitude of the polarization in future 2D systems, independent of external effects such as surface chemistry and local strains. Lateral shifts of the periodic bilayer system show a gradual evolution of the polarization when shifting between the AA, AB, and BA stacking modes, from zero to +0.33 and −0.33 Debye/nm^2, respectively (Fig. 2E). This is crucial when considering the complex response at domain walls, where lattice deformations induce additional flexo (*26*) and piezo (*27*) responses. In fig. S8, we present also the charge density redistribution in the periodic bilayer system owing to interlayer coupling. The corresponding interlayer potential difference at the experimental configuration is calculated to be $\frac{1}{2}\Delta V_{\mathrm{KP}} = 120$mV (fig. S7), in excellent agreement with the side-band measurements (red star in Fig. 2D). Similar results were reported in recent computational studies (*11*). However, to obtain quantitative agreement with the experimental measurements, the results should be carefully converged with respect to the various calculation parameters (figs. S5 and S7). By further applying an electric field of 0.1 V/nm normal to the plane, we find, from our calculations, a minute piezo-electric deformation of 0.1 pm and a 5% variation in the polarization magnitude (fig. S10).

It is instructive to further translate the measured potential difference into intralayer displacements in a simplistic point-like charges model (Δd in Fig. 1D), where each atom is allowed to displace from its layer's basal plane in the vertical direction. With the lattice site density of $n = 37\,\mathrm{nm}^{-2}$ and the on-site charge value, $q \sim e/2$, for single-layered *h*-BN (*28*, *29*), our measured ΔV_{KP} gives out-of-plane atomic displacement of the order of $\Delta d = \Delta V_{\mathrm{KP}}\varepsilon_0/4nq \sim 1 \times 10^{-3}$Å ($\varepsilon_0$ is vacuum permittivity), which is much smaller than the intralayer (1.44 Å) and interlayer (3.30 Å) spacings. This implies that the polarization is determined by a delicate competition between the various interlayer interaction components and charge redistribution. Intuitively, we expect the vdW attraction to vertically compress the nonoverlapping interfacial sites (diagonal dashed ellipse in Fig. 1D) closer together than the overlapping sites (vertical dashed ellipse in Fig. 1D), which are more prone to Pauli repulsion. This direction of motion, for example, reduces the average interlayer separation and favors Bernal (AB like) stacking in graphite over the AA configuration (*30*). In *h*-BN, however, the partial ionic nature of the two lattice sites (*12*, *31*, *32*) makes the fully eclipsed AA′ stacking more stable (*13*). Hence, imposing a polar AB interface, as in our case, may favor overlapping sites of opposite charges to come closer together than the nonoverlapping pairs and the polarization to point in the opposite direction.

To quantify these arguments, we present a reduced classical bilayer model that captures the intricate balance between Pauli, vdW, and Coulomb interatomic interactions at different stacking modes. In our model (*17*), the interfacial energy $E = \frac{1}{2}\sum_{i,j}\left[4\varepsilon\left(\left(\frac{\sigma}{r_{ij}}\right)^{12} - \left(\frac{\sigma}{r_{ij}}\right)^{6}\right) + \frac{q_i q_j}{r_{ij}}\right]$ includes a Lennard-Jones (LJ) potential characterized by the cohesive energy, ε, and the interlayer spacing scale, σ, and Coulomb interactions between the dimensionless partial atomic charges on the boron and nitrogen sites $q = \pm q_i/e$. Although neglecting any charge transfer processes between the layers that are explicitly taken into account in our DFT calculations, this model captures both the magnitude and orientation of the polarization by adjusting the ratio between ε and Coulomb scales $\propto \varepsilon/q^2$ (fig. S11). Our detailed DFT calculations indicate that in bilayer *h*-BN, the net polarization is oriented as marked by the arrows in Fig. 1D.

The permanent polarization observed in separated domains, whose dimensions can be tuned by the twist angle, each exhibiting a distinct and stable potential, may be useful in applications. To that end, however, one should identify additional ways to control the local orientation beyond the twisting mechanism. Reversible switching between AB and BA configurations, accompanied by polarization inversion, can be achieved through relative lateral translation by one atomic spacing (1.44 Å), as illustrated in Fig. 1A. Similar sliding between different stacking configurations was recently demonstrated in multilayered graphene. It was shown that both mechanical (*33*) and electric perturbations (*34*) can push domain walls, practically modifying the local stacking. In the present *h*-BN interface, however, the polar switching calls for a preferred up or down orientation that can be predetermined by the user. To obtain such a spatially resolved control, we scanned a biased tip above an individual domain to induce a local electric field normal to the interface. The polarization images before and after the biased scans are presented in Fig. 3. We observe a redistribution of domain walls to orient the local polarization with the electric field under the biased tip. For example, after scanning a negatively biased tip above the region marked by the blue square, we observed a large white domain due to the motion of the walls marked by dashed red (green) line before (after) the scan. A successive scan by a positively biased tip resulted in practically complete domain polarization flipping. Hence, by applying negative or positive bias to the tip, it is possible to determine the polarization orientation of the underlying domain. Similar switching behavior was attained above different domains within the same interface and for several measured structures (fig. S12). We note that domain-wall motion is observed for electric field values exceeding ~0.3 V/nm and when operating the biased scan in a pin-point mode (*17*).

Our results therefore demonstrate that the broken symmetry at the interface of parallel-stacked *h*-BN flakes gives rise to an out-of-plane two-dimensional polarization confined within a few interfacial layers that can be locally detected and controlled. Although the *h*-BN system, with only two different light atoms,

offers a convenient experimental and computational testbed and allows for intuitive interpretations, first-principle analysis (*11*) predicts similar phenomena to occur in other, more complex biatomic vdW crystals, such as various TMDs (*35*, *36*). Notably, the origin of the polarization and the sliding inversion mechanism presented herein are fundamentally different from the minute deformations of tightly bonded atoms in common non-centrosymmetric 3D bulk crystals. The "slidetronics" switching involves lateral motion by a full lattice spacing in a weakly coupled interface under ambient conditions. The associated sliding order parameter reveals vortices patterns around the AA points (Figs. 1C and 2B) with topological aspects resembling the hexagonal manganite system (*37*). Unlike the 3D manganites, the present 2D structure allow relaxation processes through the delamination and formation of bubbles, or the annealing of walls at the open edges (fig. S12). In the present study, however, we focus on the physics away for the domain wall and toward the domain center, where no twist, moiré pattern, or strain are considered. The sensitivity of the system to the delicate interplay between vdW attraction, Pauli repulsion, Coulomb interactions, and charge redistribution implies that external stimuli such as pressure, temperature, and/or electric fields may be used to control the polarization, thus offering many opportunities for future research.

We note that a paper in the same issue (*38*) reports similar findings. During the review process of this manuscript, similar experimental findings were also reported in (*39*), and a ferroelectric response in aligned bilayer graphene was reported in (*40*).

REFERENCES AND NOTES

1. M. Lines, A. Glass, *Principles and Applications of Ferroelectrics and Related Materials* (Oxford Univ. Press, 2001).
2. N. Setter *et al*., *J. Appl. Phys.* **100**, 051606 (2006).
3. J. F. Scott, *Ferroelectrics* **314**, 207–222 (2005).
4. J. F. Scott, *ISRN Mater. Sci.* **2013**, 1–24 (2013).
5. M. Dawber, K. M. Rabe, J. F. Scott, *Rev. Mod. Phys.* **77**, 1083–1130 (2005).
6. J. Müller, P. Polakowski, S. Mueller, T. Mikolajick, *ECS J. Solid State Sci. Technol.* **4**, N30 (2015).
7. Y. Cao *et al*., *Nano Lett.* **15**, 4914–4921 (2015).
8. D. D. Fong *et al*., *Science* **304**, 1650–1653 (2004).
9. S. S. Cheema *et al*., *Nature* **580**, 478–482 (2020).
10. F. Liu *et al*., *Nat. Commun.* **7**, 1–6 (2016).
11. L. Li, M. Wu, *ACS Nano* **11**, 6382–6388 (2017).
12. G. Constantinescu, A. Kuc, T. Heine, *Phys. Rev. Lett.* **111**, 036104 (2013).
13. R. S. Pease, *Nature* **165**, 722–723 (1950).
14. S. Zhou, J. Han, S. Dai, J. Sun, D. J. Srolovitz, *Phys. Rev. B Condens. Matter Mater. Phys.* **92**, 155438 (2015).
15. S. M. Gilbert *et al*., *2D Mater.* **6**, 021006 (2019).
16. J. H. Warner, M. H. Rümmeli, A. Bachmatiuk, B. Büchner, *ACS Nano* **4**, 1299–1304 (2010).
17. Materials, methods, and additional information are available as supplementary materials.
18. T. Maaravi, I. Leven, I. Azuri, L. Kronik, O. Hod, *J. Phys. Chem. C* **121**, 22826–22835 (2017).
19. J. S. Alden *et al*., *Proc. Natl. Acad. Sci. U.S.A.* **110**, 11256–11260 (2013).
20. M. R. Rosenberger *et al*., *ACS Nano* **14**, 4550–4558 (2020).
21. A. Weston *et al*., *Nat. Nanotechnol.* **15**, 592–597 (2020).
22. H. Yoo *et al*., *Nat. Mater.* **18**, 448–453 (2019).
23. T. A. Green, J. Weigle, *Helv. Phys. Acta* **21**, 217 (1948).
24. C. R. Woods *et al*., *Nat. Phys.* **10**, 451–456 (2014).
25. O. Hod, E. Meyer, Q. Zheng, M. Urbakh, *Nature* **563**, 485–492 (2018).
26. L. J. McGilly *et al*., *Nat. Nanotechnol.* **15**, 580–584 (2020).
27. P. Ares *et al*., *Adv. Mater.* **32**, e1905504 (2020).
28. W. M. Lomer, K. W. Morton, *Proc. Phys. Soc. A* **66**, 772–773 (1953).
29. Y.-N. Xu, W. Y. Ching, *Phys. Rev. B Condens. Matter* **44**, 7787–7798 (1991).
30. J.-C. Charlier, X. Gonze, J.-P. Michenaud, *Europhys. Lett.* **28**, 403–408 (1994).
31. N. Marom *et al*., *Phys. Rev. Lett.* **105**, 046801 (2010).
32. O. Hod, *J. Chem. Theory Comput.* **8**, 1360–1369 (2012).
33. L. Jiang *et al*., *Nat. Nanotechnol.* **13**, 204–208 (2018).
34. M. Yankowitz *et al*., *Nat. Mater.* **13**, 786–789 (2014).
35. J. Sung *et al*., *Nat. Nanotechnol.* **15**, 750–754 (2020).
36. T. I. Andersen *et al*., https://arxiv.org/abs/1912.06955 arXiv [cond-mat.mes-hall] (2019).
37. S. Artyukhin, K. T. Delaney, N. A. Spaldin, M. Mostovoy, *Nat. Mater.* **13**, 42–49 (2014).
38. K. Yasuda, X. Wang, K. Watanabe, T. Taniguchi, P. Jarillo-Herrero, *Science* **372**, 1458–1462 (2021).
39. C. R. Woods *et al*., *Nat. Commun.* **12**, 347 (2021).
40. Z. Zheng *et al*., *Nature* **588**, 71–76 (2020).
41. M. Vizner Stern *et al*., Replication Data for: Interfacial Ferroelectricity by van der Waals Sliding, Zenodo (2021).

ACKNOWLEDGMENTS

We thank Y. Lahini for useful discussions, A. Cerreta (Park Systems) for AFM support, and N. Ravid for laboratory support. We further thank J. E. Peralta for helpful discussions regarding the DFT calculations. **Funding:** W.C. acknowledges the financial support of the IASH and the Sackler Center for Computational Molecular and Materials Science at Tel Aviv University. Growth of hBN was supported by the Elemental Strategy Initiative conducted by the MEXT, Japan (grant JPMXP 0112101001), JSPS KAKENHI (grant JP20H00354), and the CREST (JPMJCR15F3), JST. E.S. acknowledges support from ARO (W911NF-20-1-0013), the Israel Science Foundation (grant 154/19, and US-Israel Binational Science Foundation (grant 2016255). M.U. acknowledges financial support of the Israel Science Foundation (grant 1141/18) and the ISFNSFC (joint grant 3191/19). O.H. is grateful for the generous financial support of the Israel Science Foundation under grant 1586/17, the Naomi Foundation for generous financial support via the 2017 Kadar Award, and the Ministry of Science and Technology of Israel under project number 3-16244. M.B.S. acknowledges funding by the European Research Council (ERC) under the European Union's Horizon 2020 research and innovation programme (grant agreement no.852925), the Israel Science Foundation (grant 1652/18), and the Israel Ministry of Science and Technology project no. 3-15619 (Meta-Materials). O.H. and M.B.S. acknowledge the Center for Nanoscience and Nanotechnology of TelAviv University. **Author contributions:** M.V.S. and Y.W. performed the experiments, supported by I.N. and supervised by M.B.S.; W.C. performed the DFT calculations supervised by M.U. and O.H.; K.W. and T.T. grew the hBN crystals; E.S. devised the adhesion model. All authors contributed to the writing of the manuscript. **Competing interests:** Ramot at Tel Aviv University Ltd. has applied for a patent (US application no. 63/083,947) on some of the technology and materials discussed here, on which M.V.S., Y.W., and M.B.S. are listed as co-inventors. **Data and materials availability:** All data needed to evaluate the conclusions in the study are present in the main text or the supplementary materials. The data have also been uploaded to Zenodo (*41*).

SUPPLEMENTARY MATERIALS

science.sciencemag.org/content/372/6549/1462/suppl/DC1
Materials and Methods
Figs. S1 to S12
Table S1
References (*42*–*59*)

16 September 2020; accepted 10 May 2021
Published online 10 June 2021
10.1126/science.abe8177

Interfacial ferroelectricity by van der Waals sliding

M. Vizner SternY. WaschitzW. CaoI. NevoK. WatanabeT. TaniguchiE. SelaM. UrbakhO. HodM. Ben Shalom

Science, 372 (6549), • DOI: 10.1126/science.abe8177

Stacking a ferroelectric

Properties of layered van der Waals structures can depend sensitively on the stacking arrangement of constituent layers. This phenomenon has been exploited to engineer superconducting, correlated insulator, and magnetic states. Two groups now show that ferroelectricity can also be engineered through stacking: Parallel-stacked bilayers of hexagonal boron nitride exhibit ferroelectric switching even though the bulk material is not ferroelectric (see the Perspective by Tsymbal). To explore these phenomena, Yasuda *et al.* used transport measurements, whereas Vizner Stern *et al.* focused on atomic force microscopy.

Science, abd3230 and abe8177, this issue p. 1458 and p. 1462; see also abi7296, p. 1389